Exacerbation of hepatic damage in endothelial aquaporin 1 transgenic mice after experimental heatstroke.

Hirokazu Ohtaki (taki@med.showa-u.ac.jp)
Showa Daigaku - Hatanodai Campus: Showa Daigaku https://orcid.org/0000-0003-3116-5265
Kazuyuki Miyamoto
Showa Daigaku - Hatanodai Campus: Showa Daigaku
Keisuke Suzuki
Showa Daigaku - Hatanodai Campus: Showa Daigaku
Motoyasu Nakamura
Showa Daigaku - Hatanodai Campus: Showa Daigaku
Hiroki Yamaga
Showa Daigaku - Hatanodai Campus: Showa Daigaku
Takuro Miyazaki
Showa Daigaku - Hatanodai Campus: Showa Daigaku
Yoshihiro Wakayama
Showa Daigaku - Hatanodai Campus: Showa Daigaku
Kazuho Honda
Showa Daigaku - Hatanodai Campus: Showa Daigaku
Kenji Dohi
Showa Daigaku - Hatanodai Campus: Showa Daigaku
Satoru Arata
Showa Daigaku - Hatanodai Campus: Showa Daigaku

Research article

Keywords: heatstroke, aquaporin 1, liver, macrophage, mouse

Posted Date: May 6th, 2021

DOI: https://doi.org/10.21203/rs.3.rs-496407/v1

Abstract

Background: Heatstroke is a life-threatening disease that causes body fluid loss and electrolyte abnormalities due to exposure to high ambient temperature (AT) and relative humidity (RH). Recently, global warming has increased the number of heatstroke patients worldwide. Aquaporin 1 (AQP1) is a water-selective protein that plays an important role in water homeostasis. However, the role of AQP1 in heatstroke has not been elucidated yet. Therefore, in this study, we examined the role of endothelial AQP1 using Tie2-Cre/LNL-AQP1 double transgenic (dTG) mice with an upregulation of *aqp1* on endothelial cells.

Methods: Tie2-Cre/LNL-AQP1 dTG mice were generated by breeding CAG-LNL(STOP)-AQP1 Tg and Tie2-Cre Tg mice. The transgenes were evaluated in the brain because brain vessels do not express *aqp1*. For production of experimental heatstroke, the mice were kept in a heatstroke chamber that was pre-heated at 41 °C AT and >99% RH for 1 h, and the blood, brain, kidney, and liver were collected 24 h later. Blood samples were analyzed for biochemical parameters such as electrolytes and tissue damage markers, and the organs were examined via morphological and immunohistological (3-nitrotyrosine (3-NT), AQP1, and Iba-1) staining.

Results: Although no difference was observed in *aqp1* expression in the whole brain, *aqp1* was detected only in Tie2-Cre/LNL-AQP1 dTG mice after capillary deprivation. Moreover, AQP1 immunostaining also revealed immunoreaction in blood vessels. After heat exposure, electrolyte abnormalities were observed in both the wild and Tie2-Cre/LNL-AQP1 dTG mice compared to non-heat stroke wild mice. Hepatic damage markers, aspartate aminotransferase and alanine aminotransferase, were increased, and serum lactate dehydrogenase levels were significantly higher in Tie2-Cre/LNL-AQP1 dTG mice than in wild mice. Hematoxylin-eosin staining and 3-NT immunoreactivity in the liver also supported hepatic damage. Moreover, the number of hepatic vasculature adherent Iba-1 positive cells was significantly higher in Tie2-Cre/LNL-AQP1 dTG mice than in wild mice.

Conclusions: In the present study, for the first time, we suggested that endothelial AQP1 contributes to hepatic damage after heatstroke.

Background

Exposure to high ambient temperature (AT) and relative humidity (RH) leads to heatstroke, which causes body fluid loss and electrolyte abnormalities. This influences water homeostasis in organs and cells, induces multiple organ damages, and progresses often to death (1). Recently, global warming has increased the incidence of heatstroke worldwide (2). In the summer of 2018 in Japan, AT presented record values, resulting in over 90,000 heatstroke-related hospitalizations and 150 deaths (https://www.fdma.go.jp/en/post1.html). In France, in the summer of 2003, over 70,000 people died due to heatstroke (3). Global warming is expected to increase in future (4, 5). Therefore, understanding the pathogeny and developing therapeutic strategies for heatstroke are important.

Aquaporins (AQPs), a family of small integral membrane proteins that facilitate the transport of water and small neutral solutes across a variety of biological membranes, are distributed in diverse organs. In mammals, 13 AQPs that regulate body fluid production, osmotic regulation, and regulation of electrolyte balance have been discovered (6). AQP1, the first identified member of the AQP isoform in the erythrocyte membrane, is known to be a water-selective transporting protein (7, 8). AQP1 is strongly expressed in the endothelial cells (ECs) of blood vessels outside the brain (9, 10), proximal tubules of the kidney (11), choroid plexus of the brain (10), inner and intralobular ducts of the pancreas, cholangiocytes of the liver, articular cartilages, and intervertebral discs (6). Although AQP1 contributes to abnormal aqueous diseases such as heatstroke, the role of AQP1 in heatstroke has not been elucidated yet.

We have recently generated Tie2-Cre/LNL-AQP1 double transgenic (Tie2-Cre/LNL-AQP1 dTG) mice using Cre/LoxP systems. An upregulation of *aqp1* on ECs under the control of Tie2 promoter has been observed (12, 13). In this study, we examined the role of endothelia AQP1 using Tie2-Cre/LNL-AQP1 dTG mice with upregulated *aqp1* on ECs. First, we confirmed the upregulation of endothelial AQP1 in the brain using reverse transcriptase PCR and immunohistochemistry. Subsequently, we subjected dTG mice to experimental heatstroke using high AT and RH to mimic the summer in temperate-to-tropical regions, including as Japan.

Methods

Animals

All animal experimental procedures involving the euthanasia were approved the Institutional Animal Care and Use Committee of Showa University (#09032) and followed by the guide line.

The mice used for generation of CAG-LNL(STOP)-AQP1 Tg mice were obtained from Sankyo Lab Service Corporation (Tokyo, Japan). C57/BL6 strained Tie2-Cre Tg mice (stock #8863) were obtained from Jackson Laboratory (Bar Harbor, ME). Tie2-Cre/LNL-AQP1 dTG mice and the wild mice littermates were obtained by the in-house breeding between CAG-LNL(STOP)-AQP1 Tg mice and Tie2-Cre Tg mice. All mice were maintained under specific pathogen-free conditions in the animal facility of Showa University under a 12-h light/dark cycle at 24 ± 2 °C, and they were kept within 10 mice in a letter size plastic animals cages, and allowed free access to food and water at least for 1 weeks for accumulation. All mated mice were euthanized by the inhalation of CO_2 between 12 to 18 months old. The other mice used for experiments were euthanized by cervical dislocation or over dose anesthesia injection described below.

CAG-LNL(STOP)-AQP1 Tg mice were generated using Cre/LoxP systems, as previously described (14). The cDNA for mouse AQP1 (831 bp) was cloned using EcoR1-Fw (gggaattcaccATGGCCAGTGAAATCAAGAAGAAGC) and Sac1-Rv (gcaggagctcCTATTTGGGCTTCATCTCCAC). Following this, the cDNA was inserted between the EcoRI and Sac1 sites of pCALNL5 vector, and the mouse AQP1 DNA was confirmed via sequencing (15). The fragments were then microinjected into 0.5-day fertilized eggs with a micromanipulator, and the eggs were transferred to the fimbriae of the uterine tubes of female Imprinting Control Region mice that were mated with vasoligated male mice 1 day before. The tails (5 mm in length) of pups (4 weeks old) were cut off, lysed with proteinase K (Wako, Tokyo, Japan), and purified with an automatic nucleic acid isolation system (Kurabo NA-2000, Tokyo, Japan) for genotyping polymerase chain reaction (PCR).

Female founders were mated with male C57BL/6 mice to confirm germline transmission using PCR genotyping and CAG-LNL(STOP)-AQP1 Tg mice were obtained. CAG-LNL(STOP)-AQP1 Tg mice were then crossed with Tie2-Cre Tg mice (stock #8863, Jackson Laboratory, Bar Harbor, ME), which carry the Cre recombinase transgene in ECs, under the control of Tie2 promoter (12, 13). This step resulted in the removal of neor cassette from the LNL-CAST transgene, thereby activating the transgenes in ECs. Tie2-Cre/LNL-AQP1 dTG mice on the B6 background were designed for *aqp1* expression in ECs. Wild-type mice were obtained from littermates.

Capillary depletion (CD) in brain and mRNA isolation

To confirm dTG mice, we checked the gene expression of *aqp1* in the brain because brain ECs generally do not express *aqp1* (9). CD was performed as previously described with minor modifications (16, 17). After cervical dislocation in male Tie2-Cre/LNL-AQP1 dTG mice and wild littermate mice, the telencephalon was freshly obtained, and the pia maters were carefully removed with a paper towel. The brain was then homogenized with 4.2 mL of capillary buffer (10 mM HEPES, 141 mM NaCl, 4 mM KCl, 2.8 mM $CaCl_2$, 1 mM NaH_2PO_4, 1 mM $MgSO_4$, 10 mM D-glucose, pH 7.4) using a loose glass dounce tissue grinder (10 strokes, Wheaton, Millville, NJ), 10.2 mL of 26 % dextran (Sigma, St Louis, MO) was added, and the mixture was gently mixed. The homogenate was centrifuged at 4,300 × g in a swing-bucket rotor for 30 min, and the supernatant was removed. The pellet was resuspended in 10 mL capillary buffer, and it was centrifuged at 8,000 × g for 30 min. The pellet was mixed with TRIzol Reagent (Invitrogen, Carlsbad, CA), and mRNA was isolated (18). The purity and concentration of extracted RNA were determined using a spectrophotometer (NanoDrop, Wilmington, DE, USA). A High-Capacity RNA-to-cDNA Kit (Applied Biosystems, Foster City, CA, USA) was used to synthesize cDNA using 2 μg total RNA, according to manufacturer's instructions. The experiment was repeated twice to check reproducibility.

PCR

PCR was performed using TaKaRa Ex Taq (TaKaRa, Shiga, Japan). The reaction mixture was prepared with an appropriate volume of cDNA mixture containing the following: 0.25 μL of forward and reverse primers (50 nmol/mL), 2.0 μL of dNTP mixture (0.25 mM each), 0.1 μL of TaKaRa Ex Taq (5 units/μL), and 2.0 μL of 10 × Ex Taq Buffer in a total volume of 20 μL. Thermal

cycling parameters were set as follows: 95 °C for 1 min for initial denaturation, 30-40 cycles at 95 °C for 45 s, 55 °C or 60 °C for 30 s, and 72 °C for 45 s. At the end of the final cycle, an additional 7-min extension step was performed at 72 °C. Ten microliters of each reaction mixture was electrophoresed on a 2.0 % agarose gel, and the bands were visualized using ethidium bromide. Mouse ribosomal protein S18 (*rps18*) was used as the housekeeping gene. The primers are shown in Table 1.

Table 1 List of Primers

Gene symbol	Amplicon size	Fwd	Rev	Ref Seq numbers
Aqp1	124	AGGCTTCAATTACCCACTGGA	GTGAGCACCGCTGATGTGA	NM_007472
Pecam	136	TGGTTGTCATTGGAGTGGTC	TTCTCGCTGTTGGAGTTCAG	NM_008816
Pecam	812	GGTGACCTCCAATGACCCAG	GCCTTCCGTTCTTAGGGTCG	NM_008816
vwf	125	CTTCTGTACGCCTCAGCTATG	GCCGTTGTAATTCCCACACAAG	NM_011708.4
Eno2	302	TGAGAATAAATCCTTGGAGCTGGT	GGTCATCGCCCACTATCTGG	NM_001302642
Gfap	419	CTAACGACTATCGCCGCCAA	CTGGTGAGCCTGTATTGGGAC	NM_001131020
Mbp	262	CAGAGTCCGACGAGCTTCAG	CAGCTTCTCTACGGCTCGG	NM_001025245
Aif1	144	ATCAACAAGCAATTCCTCGATGA	CAGCATTCGCTTCAAGGACATA	NM_019467
Rps18	166	AGTTCCAGCACATTTTGCGAG	TCATCCTCCGTGAGTTCTCCA	NM_011296

Foot note, All primers were obtained from Eurofins Genomics (Tokyo, Japan).

Multiple-staining for AQP1 localization

To visualize AQP1 on ECs in the brain, we examined the *in situ* labeling of ECs with tomato-lectin and multiple immunostaining. Following an overdose of sodium pentobarbital (100 mg/kg, i.p.) anesthesia, the male Tie2-Cre/LNL-AQP1 dTG mice and wild littermate mice (n=3) aged 11 month olds were transcardially perfused with 0.9% NaCl to remove blood, and subsequently, 1% paraformaldehyde was injected. The mice were then perfused with 10 mL of 5 μg/mL DyLight 488-labeled Lycopersicon Esculentum (Tomato) lectin (Vector Lab, Burlingame, CA), and the brain was collected. The brain was immersed in 20% sucrose in 0.1 M phosphate buffer (pH 7.2; PB) for two nights, and it was embedded in liquid nitrogen-cooled isopentane using an embedding solution (20% sucrose in 0.1 M PB: O.C.T. compound (Sakura Finetech, Tokyo, Japan, 2:1). Coronal sections (thickness, 8 μm) were obtained using a cryostat (Hyrax50, Carl Zeiss, Oberkochen, Germany), and they were immunostained.

After washing with PBS, the sections were subjected to heat-mediated antigen retrieval with 10 mM sodium citrate (pH 6.0) at 95 °C for 25 min. The sections were washed with phosphate-buffered saline (PBS) containing 0.05% Tween 20 (PBST), and they were incubated with MOM mouse IgG blocking (Vector Lab). The sections were blocked with 5% normal horse serum (NHS, Vector) for 60 min, and subsequently, they were incubated with mouse anti-rat AQP1 (1/22) (1:200, Santa Cruz Biotechnology, Santa Cruz, CA) and/or rabbit anti-GFAP (1:10, DAKO, Glostrup, Denmark) antibodies at 4 °C overnight. The sections were incubated with appropriate Alexa labeled secondary antibodies at room temperature for 2 h. The cell nuclei were stained with 4,6-diamidine-2-phenylindole dihydrochloride (1:10,000; Roche, Manheim, Germany) for some cases, and they were incubated in 1.0 mM $CuSO_4$ in 50 mM ammonium acetate buffer (pH 5.0) to diminish autofluorescence (19). Fluorescence was detected using an Axio Imager optical sectioning microscope with ApoTome (Carl Zeiss).

Heatstroke model

The acrylic semi-enclosed heatstroke chamber (200 mm × 340 mm × 300 mm) was originally produced by placing one animal cage on top of another, similar to a greenhouse (20). An ultrasonic humidifier (USB-68, Sanwa, Okayama, Japan) and a digital thermo-hygrometer (AD-5696, A&D Company, Tokyo, Japan) were used for humidification and monitoring of AT, RH, and wet bulb

globe temperature (WBGT). WBGT is an environmental index that accounts for AT and RT in a room (21, 22), and it recommends the use of International Labour Organization to evaluate the environment of workers (https://www.ilo.org). The heatstroke chamber was placed in an incubator (Bio-chamber, BCP-120F, TITEC, Aichi, Japan), which was pre-heated at 41 °C AT and >99% RH for 3 h or more.

Three hours prior to heat exposure, the male mice aged 11 month olds were weighed and dehydrated. Following this, the mice were placed in a heatstroke chamber for 60 min, and they were returned to room temperature (23 ± 1 °C) with free access to food and water. Body weights (BWs) were measured four times before dehydration, immediately before/after heat exposure, and after 24 h of heat exposure. Nine mice (four wild and five Tie2-Cre/LNL-AQP1 dTG mice) were subjected to heat exposure.

After twenty-four hours of 1 h heat exposure, the mice were anesthetized with an overdose of sodium pentobarbital (100 mg/kg, i.p.). Blood samples were collected from the right ventricle of the heart, and the mice were transcardially perfused with 0.9% NaCl and 10% neutralized formalin. Blood samples were centrifuged at 1,500 × g for 10 min to collect the serum. Serum samples were examined for biochemical parameters. Fixed organs, such as the liver, kidney, and brain, were collected, paraffin-embedded 4 μm-thick sections were prepared, and morphohistological changes were evaluated.

Serum biochemical parameters

Serum levels of total protein (TP), albumin (ALB), total bilirubin (T-bil), aspartate aminotransferase (AST), alanine aminotransferase (ALT), alkaline phosphatase (ALP), lactate dehydrogenase (LDH), creatinine kinase (CK), blood urea nitrogen (BUN), creatinine (Cre), electrolytes (Na^+, K^+, and Cl^-), glucose, lactate (LA), and osmotic pressure were analyzed. TP was analyzed using the biuret method; ALB was analyzed using the BCG method; BUN was analyzed using the urease-GLDH method; T-bil, Cre, and LA were analyzed using the enzymatic method; AST, ALT, ALP, LDH, and CK were analyzed using the MDH-UV method; electrolytes were analyzed using the ion selective electrode method; and osmotic pressure was analyzed using the freezing point depression method. All assays were performed using a HITACHI 7180 (Hitachi, Tokyo, Japan).

Immunohistochemistry and cell counts

Paraffin-embedded sections were deparaffinized using a series of concentrations of xylene and alcohol, and they were subjected to hematoxylin-eosin and immunohistochemical staining.

After washing with PBS, the sections were subjected to heat-mediated antigen retrieval with 10 mM sodium citrate buffer (pH 6.0) at 95 °C for 25 min, and subsequently, they were immersed in 0.3 % H_2O_2/MeOH for 30 min. For AQP1 immunostaining, the sections were incubated with MOM mouse IgG blocking. The sections were blocked with non-specific binding with 5% NHS, and they were incubated with rabbit anti-Iba1 (1:500, Wako), rabbit anti-3-nitrotyrosine (1:500, Upstate Biotechnology, Lake Placid, NY), or mouse anti-rat AQP1 (1/22) (1:200) antibodies at 4 °C overnight. The sections were incubated with either biotinylated goat anti-rabbit (Invitrogen) or anti-mouse IgG (DAKO) secondary antibodies for 2 h. They were then incubated in an avidin-biotin complex solution (Vector) and diaminobenzidine (Sigma), a chromogen. Sections were observed under a microscope (Olympus BX53; Olympus, Tokyo, Japan), and images were captured with an Olympus cellSens standard 2.1 (Olympus). Staining was conducted on sections obtained from 4 and 5 wild-type and Tie2-Cre/LNL-AQP1 dTG mice, respectively.

To determine the influence of AQP1 on monocyte / macrophage infiltration, we manually counted the number of monocytes / macrophages attached to the vasculature after Iba1-immunostaining in the brain, liver, and kidney using the process mode in Olympus cellSens standard 2.1. The number of Iba1-positive immunoreactions was counted in 30 vessels of the telencephalons and livers and 20-24 vessels in the kidneys from 3-4 to sections in each mouse. The boundary length of counted vessels was measured, and the estimated diameter of each vessel was calculated. The cells were counted in small-and medium-sized vessels, and they were not counted in capillaries, including sinusoids of the liver. An investigator (M.N. and H.Y.) who was blinded to the mouse genotype performed the counting.

Statistical analysis

Data are expressed as the mean ± standard error of the mean. Statistical comparisons were conducted using one-way analyses of variance following non-parametric multiple comparisons, as indicated in each figure legend. A value of $p<0.05$ was considered statistically significant. Analyses were performed using Bell Curve for Excel (Bell Curve, Tokyo, Japan).

Results

Evaluation of Tie2-Cre/LNL-AQP1 dTG mice

AQP1 was first identified in erythrocyte membranes (23) and is expressed in the kidneys, lungs, heart, liver, cornea, blood vessels, cornea, and choroid plexus (6). However, it is not usually expressed in brain blood vessels (9). Therefore, we examined *aqp1* expression in the capillaries of telencephalon in the brain. We evaluated the specificity of Tie2-Cre/LNL-AQP1 dTG mice. *Aqp1* expression was similarly detected in whole brain homogenates of both wild-type and Tie2-Cre/LNL-AQP1 dTG mice (Figure. 1a). However, after collecting the cerebral vasculature (CD fraction), *aqp1* expression could accurately detect signals in Tie2-Cre/LNL-AQP1 dTG mice but not in wild mice. Since the vasculature transcriptomes, *pecam* (two sets of primers) and *vwf*, were similarly expressed in both animals, the brain in Tie2-Cre/LNL-AQP1 dTG mice suggested an increase in *aqp1* expression. Moreover, CD fraction showed a lower expression of neuronal or glial transcriptomes, such as *eno2*, *gfap*, *mbp*, and *aif1*, than the whole brain fraction. It also indicated that the brain in Tie2-Cre/LNL-AQP1 dTG mice showed an increased vasculature *aqp1* expression. We then observed the stained brain sections for AQP1 antibody (Figures. 1b and c). AQP1-immunoreactions (-ir) in wild mice were observed in the neuronal layer of piriform cortex. However, AQP1-ir in Tie2-Cre/LNL-AQP1 dTG mice was observed in vasculature-like structures as well as in the neuronal layer of cortex. Following this, we examined the *in situ* vasculature with tomato-lectin, and we performed multiple staining of AQP1. Although AQP1-ir in the wild mice was weakly observed in the same field with higher magnification, AQP1-ir did not merge with tomato-lectin signals and it mostly merged with GFAP-ir. On the other hand, in Tie2-Cre/LNL-AQP1 dTG mice, AQP1-ir was merged with tomato-lectin signals, indicating its expression on ECs (Figure. 1c).

Changes in AT, RH, and WBGT during heat exposure

We exposed the animals to experimental heatstroke, which were subjected to high AT and RH for 60 min. Figure. 2a shows trends in AT, RH, and WBGT in the semi-enclosed heatstroke chamber. During 3 h of incubation and before heat exposure, AT and RH values inside the chamber were 38.1 °C and >99.9 %, respectively, and WBGT was calculated at 42.0 °C. Although these conditions temporally decreased when the animals were dropped into the chamber, AT and WBGT gradually increased and finally reached 39.9 °C and 43.9 °C after 60 min. The animals exhibited jumping at approximately 40 min after exposure and/or gathering at the corner of the chamber. However, no animals died for 60 min during heat exposure and 1 day following recovery. Changes in BW during the experimental period are shown in Figure. 2b. Compared to prior hydration, BW decreased to approximately 96.5 % after heat exposure, and it returned to basal level 1 day after heat exposure. No significant difference was observed between the groups.

Serum biochemical parameters after 1 day of heat exposure

The electrolytes, such as Na^+, K^+, and Cl^-, and osmotic pressures are shown in Figure. 3. To confirm electrolyte abnormalities after heat exposure, Na^+ and K^+ were decreased and Cl^- was increased in both experimental groups compared to that in non-heat-exposed wild animals. Significant differences were observed for all electrolytes in wild mice and for Cl^- in Tie2-Cre/LNL-AQP1 dTG mice after heat exposure compared to non-heat-exposed wild animals; however, no difference was observed between the heat expose groups.

Next, we determined tissue damage markers in the serum after heat exposure (Figure. 4). Most of them were not significantly different between the wild and Tie2-Cre/LNL-AQP1 dTG mice after heat exposure. However, LDH, a tissue damage marker, was significantly higher in Tie2-Cre/LNL-AQP1 dTG mice than in wild-type mice ($p<0.05$). Moreover, hepatic damage markers, ALT and AST, increased in Tie2-Cre/LNL-AQP1 dTG mice; however, the difference was not significant. These results suggest that Tie2-Cre/LNL-AQP1 dTG mice could increase tissue damage, probably hepatic damage, as compared to wild mice after heat exposure.

Increase in inflammation in the liver of Tie2-Cre/LNL-AQP1 dTG mice

We compared hepatic morphological alterations between the wild and Tie2-Cre/LNL-AQP1 dTG mice after heat exposure (Figure. 5). Hepatocytes in the non-heat exposure wild mice exhibited large and round nuclei, with distinct outline. The sinusoid radiated outward from the central vein. After heat exposure, the nuclei in the hepatocytes of wild mice somewhat shrank, and they were deeply stained. The sinusoids were still recognized radially, and few leukocytes were also observed. After heat exposure, the hepatic lobules in Tie2-Cre/LNL-AQP1 dTG mice had a fuzzy sinusoid arrangement, and many leukocytes were observed. The nuclei in the hepatocytes shrank, and they were deeply stained. Morphological observations suggested that the hepatic tissues in Tie2-Cre/LNL-AQP1 dTG mice were inflamed.

Increase in oxidative stress in Tie2-Cre/LNL-AQP1 dTG mice

To confirm hepatic damage, a proteinic oxidative metabolite, 3-NT, was immunostained in the liver (Figure. 6). Minimal or no staining was observed in the primary antibody-free negative control staining in the livers of Tie2-Cre/LNL-AQP1 dTG mice. 3-NT-ir was slightly detected in wild mice, and it was prominent in the vessels, including sinusoids of the livers of Tie2-Cre/LNL-AQP1 dTG mice. This result also supported the increased hepatic damage in Tie2-Cre/LNL-AQP1 dTG mice.

Expression of hepatic AQP1 on vessels

We then determined the localization of AQP1 in the liver after 24 h of heat exposure (Figure. 7). AQP1-ir was ubiquitously expressed in the hepatic vasculature, including the sinusoids of non-heat-exposed wild mice, and AQP1-ir showed no staining in the hepatocytes and small bile ducts of portal triads. AQP1-ir staining was not drastically different between the wild and Tie2-Cre/LNL-AQP1 dTG mice after heat exposure.

Increase in Iba1-positive cells on vessels in the liver of Tie2-Cre/LNL-AQP1 dTG mice

Next, we stained the hepatic tissues with an anti-Iba1 antibody (Figure. 8). Iba1 is a marker of monocytes/macrophages. Iba1-ir did not drastically differ in the sinusoids between the wild and Tie2-Cre/LNL-AQP1 dTG mice, suggesting the presence of Kupffer cells (Figures. 8a and b). However, Iba1-ir was highly noticeable on the small-and medium-sized vessels in Tie2-Cre/LNL-AQP1 dTG mice (Figures. 8c-f). The number of vasculatures that adhered to $Iba1^+$ in the liver was counted among the groups. Moreover, to compare the livers, $Iba1^+$ numbers were counted in the telencephalic vessels in the brain and interlobal to interlobular vessels in the kidneys (Fig. 9). Generally, the brain does not express AQP1 in wild mice, as shown in Fig. 1, and the kidney is a critical tissue for water homeostasis. $Iba1^+$ numbers on the hepatic vessels of wild mice with/without heat exposure were counted, and they were 1.76 ± 0.16 and 2.55 ± 0.53/mm, respectively. $Iba1^+$ number on the hepatic vessels of Tie2-Cre/LNL-AQP1 dTG mice was 5.36 ± 1.45 ($p<0.01$), and it was significantly greater than that of the wild mice both with/without heat exposure (Figure. 9a). In contrast, the numbers in the brains and kidneys were less than 2.2/mm in all groups, and they were not significantly different (Figures. 9b and c).

To determine the role of AQP1 in hepatic vessels, the relationship between $Iba1^+$ cells and vessel diameter was determined between the wild and Tie2-Cre/LNL-AQP1 dTG mice (Figure. 9d). While $Iba1^+$ numbers showed a greater trend in all sizes of vessels in Tie2-Cre/LNL-AQP1 dTG mice than in wild mice, $Iba1^+$ numbers were significantly greater in Tie2-Cre/LNL-AQP1 dTG mice, in particular, in relatively small vessels (0 - 150 and 150 - 300 μm), as compared to that in heat-exposed wild mice.

Discussions

AQP1 is a water-selective transport protein that plays an important role in fluid production, osmotic regulation, and electrolyte balance (6). Heatstroke causes body fluid loss and electrolyte abnormalities due to exposure to high AT and RH (1), and appropriate rehydration to maintain osmotic and electrolyte balance is an important strategy to decrease the risk of heatstroke (20). However, the role of AQP1 in heatstroke has not been determined yet. In the present study, we generated Tie2-Cre/LNL-AQP1 dTG mice using Cre/LoxP systems with an upregulation of *aqp1* on ECs under the control of Tie2 promoter. The mice were then subjected to experimental heatstroke by exposing them to high AT and RH to evaluate the role of vasculature AQP1. To confirm

the genetic modification of Tie2-Cre/LNL-AQP1 dTG mice, we first determined the telencephalic AQP1 level because the ECs in the brain do not express AQP1 (9).

Aqp1 expression in the whole brain of both wild-type and Tie2-Cre/LNL-AQP1 dTG mice was similar. However, after CD, *aqp1* expression was detected only in Tie2-Cre/LNL-AQP1 dTG mice while the levels of endothelial marker genes, *pecam* and *vwf,* were similar in both the wild and Tie2-Cre/LNL-AQP1 dTG mice. Moreover, immunostaining for AQP1 also supported these results. In the brain, AQP1 is known to localize strongly in the apical membrane of choroid plexus (24), neurons, and astrocytes (6, 25). Immunostaining revealed that the neuronal layers of piriform cortex and astrocytes, which show very low intensity, were also recognized as AQP1-ir. The brains of Tie2-Cre/LNL-AQP1 dTG mice showed a clearly labeled vasculature-like structure that merged with ECs.

In the present study, initially, the mice were exposed to AT and RH of 38.1 °C and >99.9%, respectively, and after 60 min, AT and RH became 39.9 °C and >99.9 %, respectively. WBGT was calculated at 42.0 °C and 43.9 °C. In Japan, a WBGT of more than 31 °C is considered dangerous for human health (https://www.wbgt.env.go.jp/en/wbgt.php). Therefore, heat stress is considered to be extremely severe and sub-lethal. After heat exposure, the wild and Tie2-Cre/LNL-AQP1 dTG mice showed a 3 – 4 % decrease in body weight, with no significant difference. Serum Na^+ and K^+ levels decreased and Cl^- increased in Tie2-Cre/LNL-AQP1 dTG mice than in non-heat-exposed wild mice, and no difference was observed between the wild and Tie2-Cre/LNL-AQP1 dTG mice after heat exposure. Although the osmotic pressures were different after heat exposure due to large deviations, the heat-exposed animals showed early symptoms of heatstroke (1).

We compared the serum biochemical parameters, and we observed that the cellular damage marker LDH was significantly higher in Tie2-Cre/LNL-AQP1 dTG mice than in wild mice. Moreover, hepatic damage markers, AST and ALT, also increased in Tie2-Cre/LNL-AQP1 dTG mice; however, the increase was not significant. Therefore, we further analyzed hepatic morphology. The hepatic morphology and oxidative stress detected by 3-NT-ir also suggested hepatic impairment in Tie2-Cre/LNL-AQP1 dTG mice.

No study has reported the role of AQP1 in heatstroke. However, some studies have suggested its role in hepatic damage. AQP1 expression is increased in liver ECs in cirrhosis via bile duct ligation. AQP1 gene deficient (KO) mice with cirrhosis showed decreased angiogenesis, fibrosis, and portal hypertension, which depends on the osmotically sensitive microRNA to AQP1 pathway (26-28). These results are consistent with our results, suggesting that an increased expression of AQP1 in ECs deteriorates hepatic injury. The caspase-3 inhibitor prevented pulmonary injury induced by common bile duct ligation, which is an experimental model of hepatopulmonary syndrome, and it decreased apoptosis and endothelial AQP1 levels (29). Fibroblasts obtained from gene-deficient mice with N-glycanase 1 and human gene-silencing fibroblasts decreased *aqp*1, and they were resistant to hypotonic lysis (30).

In contrast, some reports have shown that AQP1 induction decreases inflammation and apoptosis in hepatic and pulmonary injuries. Hepatocyte-induced AQP1 using adenovirus improves estrogen-induced and lipopolysaccharide-induced cholestasis in rats (31-33). Alpinetin, a Chinese medicine, alleviates lung AQP1 levels (34). Induction of a flow-responsive transcription factor, Krüppel-like factor 2 (KLF2), *in vitro* is accompanied by AQP1 induction. KLF2 maintains an anti-coagulant and anti-inflammatory endothelium with sufficient nitric oxide bioavailability. Thus, an endothelial expression of AQP1 characterizes the atheroprotected, non-inflamed vessel wall (35).

In the present study, we generated mice that highly expressed AQP1 on ECs, and AQP1 immunostaining was also expressed in the intralobular vessels and sinusoids but not in the hepatocytes and intralobular bile ducts of portal triads. Together these results suggest that endothelial AQP1 increment might contribute to hepatic injury, depending on electrolyte abnormalities and osmotic changes.

The role of AQP1 in human heatstroke patients needs further investigation because the localization of AQP1 in the liver can exist in a species difference. The localization of AQP1 in rodents has mainly been reported in ECs, but the levels are minimal or low in the bile ducts and hepatocytes (26-28), similar to our results. However, AQP1 localization in pigs and humans is not only

observed in the vessels, also in the bile ducts and hepatocytes (36, 37) and AQP1 is more dominant in bile ducts than in vessels (38, 39).

Finally, we observed that vasculature-adherent Iba-1$^+$ monocytes/macrophages increased in the small and medium sized intralobular vessels of Tie2-Cre/LNL-AQP1 dTG mice, but they were not prominent in sinusoidal Iba-1$^+$ cells, Kupffer cells. An increase in the number of Iba-1$^+$ cells in Tie2-Cre/LNL-AQP1 dTG mice was not observed in the telencephalic and renal vessels. These results also suggest that an increased hepatic damage in Tie2-Cre/LNL-AQP1 dTG mice can induce the migration of monocytes/macrophages. In particular, Iba-1$^+$ monocytes/macrophages in Tie2-Cre/LNL-AQP1 dTG mice were significantly greater in small vessels, probably due to an impairment in hepatic circulation because the sinusoids in Tie2-Cre/LNL-AQP1 dTG mice were unclear and partially obstructed. Expression of endothelial AQP1 might also correlate with the induction of endothelial adhesion molecules and acquisition of circulating leukocytes. Myocardin-related transcription factor-A KO mice showed a significantly attenuated neointima formation and decreased expression of *aqp1*. Moreover, the expression of *icam1*, *mmp9*, and *itgb1* decreases in KO mice (40). Single nucleotide polymorphisms in the priapism in patients with sickle cell disease are associated with TGFBR3, AQP1, and integrin-αv (41). Further studies are needed to clarify the properties of hepatic vessels and AQP1 after heatstroke.

Conclusions

In the present study, we genetically generated Tie2-Cre/LNL-AQP1 dTG mice with upregulated *aqp1* on ECs under the control of Tie2 promoter. After a severe heat exposure, although both the wild and Tie2-Cre/LNL-AQP1 dTG mice exhibited electrolyte abnormalities, Tie2-Cre/LNL-AQP1 dTG mice showed a significantly increased liver injury, 3-NT levels, and hepatic vasculature adherent monocyte/macrophages. These results suggest that an increase in endothelial AQP1 plays an important role in hepatic inflammation.

List Of Abbreviations

ALB: albumin

ALP: alkaline phosphatase

ALT: alanine aminotransferase

AQP: aquaporin

AST: aspartate aminotransferase

AT: ambient temperature

BUN: blood urea nitrogen

BW: body weights

CD: capillary depletion

CK: creatinine kinase

Cre: creatinine

EC: endothelial cell

Ir: immunoreactions

KLF2: Krüppel-like factor 2

KO mice: gene deficient mice

LA: lactate

LDH: lactate dehydrogenase

PB: phosphate buffer

PBST: phosphate-buffered saline containing 0.05% Tween 20

PCR: polymerase chain reaction

RH: relative humidity

T-bil: total bilirubin

TP: total protein

WBGT: wet bulb globe temperature

Declarations

Ethics approval and consent to participate

All experimental procedures involving animals were approved by the Institutional Animal Care and Use Committee of Showa University (#09032)

Consent for publication

Not applicable.

Availability of data and materials

The datasets generated for this study are available on request from the corresponding author

Competing interests

The authors declare that the study was conducted in the absence of any commercial or financial relationships that could be construed as a potential conflict of interest.

Funding

This work was supported by JSPS KAKENHI Grant-in-Aid for Exploratory Research Number 19K22779 (Kenji Dohi) and Grant-in-Aid for Scientific Research (C) Number 19K09442 (Kazuyuki Miyamoto) from the Japan Society for the Promotion of Science. These funders had no role in the design of the study and collection, analysis, and interpretation of data and in writing the manuscript.

Authors' contributions

HO, KM, and SA contributed to study conception and design. HO, KM, KS, MN, and HY performed the experiments. TM, YW, and AS provided the experimental resources. KM and KD performed the funding acquisition. KH supervised the pathological observations. HO wrote the first draft of this manuscript. KM, TM, YW, and SA wrote sections of the manuscript. All authors contributed to manuscript revision and reading, and all of them approved the submitted version.

Acknowledgements

We also would like to thank Editage (https://app.editage.jp) for English language editing.

References

1. Epstein Y, Yanovich R. Heatstroke. N Engl J Med. 2019;380(25):2449-59.
2. Sharma HS, Westman J, Nyberg F. Pathophysiology of brain edema and cell changes following hyperthermic brain injury. Prog Brain Res. 1998;115:351-412.
3. Robine JM, Cheung SL, Le Roy S, Van Oyen H, Griffiths C, Michel JP, et al. Death toll exceeded 70,000 in Europe during the summer of 2003. C R Biol. 2008;331(2):171-8.
4. Sherwood SC, Huber M. An adaptability limit to climate change due to heat stress. Proc Natl Acad Sci U S A. 2010;107(21):9552-5.
5. Meehl GA, Tebaldi C. More intense, more frequent, and longer lasting heat waves in the 21st century. Science. 2004;305(5686):994-7.
6. Day RE, Kitchen P, Owen DS, Bland C, Marshall L, Conner AC, et al. Human aquaporins: regulators of transcellular water flow. Biochim Biophys Acta. 2014;1840(5):1492-506.
7. Agre P, Saboori AM, Asimos A, Smith BL. Purification and partial characterization of the Mr 30,000 integral membrane protein associated with the erythrocyte Rh(D) antigen. J Biol Chem. 1987;262(36):17497-503.
8. Agre P, King LS, Yasui M, Guggino WB, Ottersen OP, Fujiyoshi Y, et al. Aquaporin water channels--from atomic structure to clinical medicine. J Physiol. 2002;542(Pt 1):3-16.
9. Papadopoulos MC, Verkman AS. Aquaporin water channels in the nervous system. Nat Rev Neurosci. 2013;14(4):265-77.
10. Oshio K, Watanabe H, Song Y, Verkman AS, Manley GT. Reduced cerebrospinal fluid production and intracranial pressure in mice lacking choroid plexus water channel Aquaporin-1. FASEB J. 2005;19(1):76-8.
11. Ishibashi K, Sasaki S, Fushimi K, Uchida S, Kuwahara M, Saito H, et al. Molecular cloning and expression of a member of the aquaporin family with permeability to glycerol and urea in addition to water expressed at the basolateral membrane of kidney collecting duct cells. Proc Natl Acad Sci U S A. 1994;91(14):6269-73.
12. Sakai K, Miyazaki J. A transgenic mouse line that retains Cre recombinase activity in mature oocytes irrespective of the cre transgene transmission. Biochem Biophys Res Commun. 1997;237(2):318-24.
13. Kisanuki YY, Hammer RE, Miyazaki J, Williams SC, Richardson JA, Yanagisawa M. Tie2-Cre transgenic mice: a new model for endothelial cell-lineage analysis in vivo. Dev Biol. 2001;230(2):230-42.
14. Sato H, Kato R, Isogai Y, Saka G, Ohtsuki M, Taketomi Y, et al. Analyses of group III secreted phospholipase A2 transgenic mice reveal potential participation of this enzyme in plasma lipoprotein modification, macrophage foam cell formation, and atherosclerosis. J Biol Chem. 2008;283(48):33483-97.
15. Kanegae Y, Takamori K, Sato Y, Lee G, Nakai M, Saito I. Efficient gene activation system on mammalian cell chromosomes using recombinant adenovirus producing Cre recombinase. Gene. 1996;181(1-2):207-12.
16. Pan W, Banks WA, Kastin AJ. Permeability of the blood-brain and blood-spinal cord barriers to interferons. J Neuroimmunol. 1997;76(1-2):105-11.
17. Pan W, Ding Y, Yu Y, Ohtaki H, Nakamachi T, Kastin AJ. Stroke upregulates TNFalpha transport across the blood-brain barrier. Exp Neurol. 2006;198(1):222-33.
18. Yagura K, Ohtaki H, Tsumuraya T, Sato A, Miyamoto K, Kawada N, et al. The enhancement of CCL2 and CCL5 by human bone marrow-derived mesenchymal stem/stromal cells might contribute to inflammatory suppression and axonal extension after spinal cord injury. PLoS One. 2020;15(3):e0230080.
19. Schnell SA, Staines WA, Wessendorf MW. Reduction of lipofuscin-like autofluorescence in fluorescently labeled tissue. J Histochem Cytochem. 1999;47(6):719-30.
20. Miyamoto K, Suzuki K, Ohtaki H, Nakamura M, Yamaga H, Yagi M, et al. A novel mouse model of heatstroke accounting for ambient temperature and relative humidity. J Intensive Care. 2021 (*in press*)
21. YAGLOU CP, MINARD D. Control of heat casualties at military training centers. AMA Arch Ind Health. 1957;16(4):302-16.

22. Ramanathan NL, Belding HS. Physiologic evaluation of the WBGT index for occupational heat stress. Am Ind Hyg Assoc J. 1973;34(9):375-83.
23. Preston GM, Agre P. Isolation of the cDNA for erythrocyte integral membrane protein of 28 kilodaltons: member of an ancient channel family. Proc Natl Acad Sci U S A. 1991;88(24):11110-4.
24. Obata F, Narita K. Hypercholesterolemia negatively influences morphology and molecular markers of epithelial cells within the choroid plexus in rabbits. Fluids Barriers CNS. 2020;17(1):13.
25. Satoh J, Tabunoki H, Yamamura T, Arima K, Konno H. Human astrocytes express aquaporin-1 and aquaporin-4 in vitro and in vivo. Neuropathology. 2007;27(3):245-56.
26. Huebert RC, Vasdev MM, Shergill U, Das A, Huang BQ, Charlton MR, et al. Aquaporin-1 facilitates angiogenic invasion in the pathological neovasculature that accompanies cirrhosis. Hepatology. 2010;52(1):238-48.
27. Huebert RC, Jagavelu K, Hendrickson HI, Vasdev MM, Arab JP, Splinter PL, et al. Aquaporin-1 promotes angiogenesis, fibrosis, and portal hypertension through mechanisms dependent on osmotically sensitive microRNAs. Am J Pathol. 2011;179(4):1851-60.
28. Yokomori H, Oda M, Yoshimura K, Watanabe S, Hibi T. Aberrant expressions of aquaporin-1 in association with capillarized sinusoidal endothelial cells in cirrhotic rat liver. Med Mol Morphol. 2010;43(1):6-12.
29. Chen B, Ning JL, Gu JT, Cui J, Yang Y, Wang Z, et al. Caspase-3 inhibition prevents the development of hepatopulmonary syndrome in common bile duct ligation rats by alleviating pulmonary injury. Liver Int. 2015;35(4):1373-82.
30. Tambe MA, Ng BG, Freeze HH. N-Glycanase 1 Transcriptionally Regulates Aquaporins Independent of Its Enzymatic Activity. Cell Rep. 2019;29(13):4620-31.e4.
31. Marrone J, Lehmann GL, Soria LR, Pellegrino JM, Molinas S, Marinelli RA. Adenoviral transfer of human aquaporin-1 gene to rat liver improves bile flow in estrogen-induced cholestasis. Gene Ther. 2014;21(12):1058-64.
32. Marrone J, Soria LR, Danielli M, Lehmann GL, Larocca MC, Marinelli RA. Hepatic gene transfer of human aquaporin-1 improves bile salt secretory failure in rats with estrogen-induced cholestasis. Hepatology. 2016;64(2):535-48.
33. Marrone J, Danielli M, Gaspari CI, Marinelli RA. Adenovirus-mediated human aquaporin-1 expression in hepatocytes improves lipopolysaccharide-induced cholestasis. IUBMB Life. 2017;69(12):978-84.
34. Liang X, Zhang B, Chen Q, Zhang J, Lei B, Li B, et al. The mechanism underlying alpinetin-mediated alleviation of pancreatitis-associated lung injury through upregulating aquaporin-1. Drug Des Devel Ther. 2016;10:841-50.
35. Fontijn RD, Volger OL, van der Pouw-Kraan TC, Doddaballapur A, Leyen T, Baggen JM, et al. Expression of Nitric Oxide-Transporting Aquaporin-1 Is Controlled by KLF2 and Marks Non-Activated Endothelium In Vivo. PLoS One. 2015;10(12):e0145777.
36. Talbot NC, Garrett WM, Caperna TJ. Analysis of the expression of aquaporin-1 and aquaporin-9 in pig liver tissue: comparison with rat liver tissue. Cells Tissues Organs. 2003;174(3):117-28.
37. Yokomori H, Oda M, Yoshimura K, Kaneko F, Hibi T. Aquaporin-1 associated with hepatic arterial capillary proliferation on hepatic sinusoid in human cirrhotic liver. Liver Int. 2011;31(10):1554-64.
38. Iguchi H, Oda M, Yamazaki H, Yoshimura K, Ando W, Yokomori H. Aquaporin-1 is associated with arterial capillary proliferation and hepatic sinusoidal transformation contributing to portal hypertension in primary biliary cirrhosis. Med Mol Morphol. 2014;47(2):90-9.
39. Marinelli RA, Gradilone SA, Carreras FI, Calamita G, Lehmann GL. Liver aquaporins: significance in canalicular and ductal bile formation. Ann Hepatol. 2004;3(4):130-6.
40. Jiang Y. The expression of MRTF-A and AQP1 play important roles in the pathological vascular remodeling. Asian Pac J Cancer Prev. 2015;16(4):1375-83.
41. Elliott L, Ashley-Koch AE, De Castro L, Jonassaint J, Price J, Ataga KI, et al. Genetic polymorphisms associated with priapism in sickle cell disease. Br J Haematol. 2007;137(3):262-7.

Figures

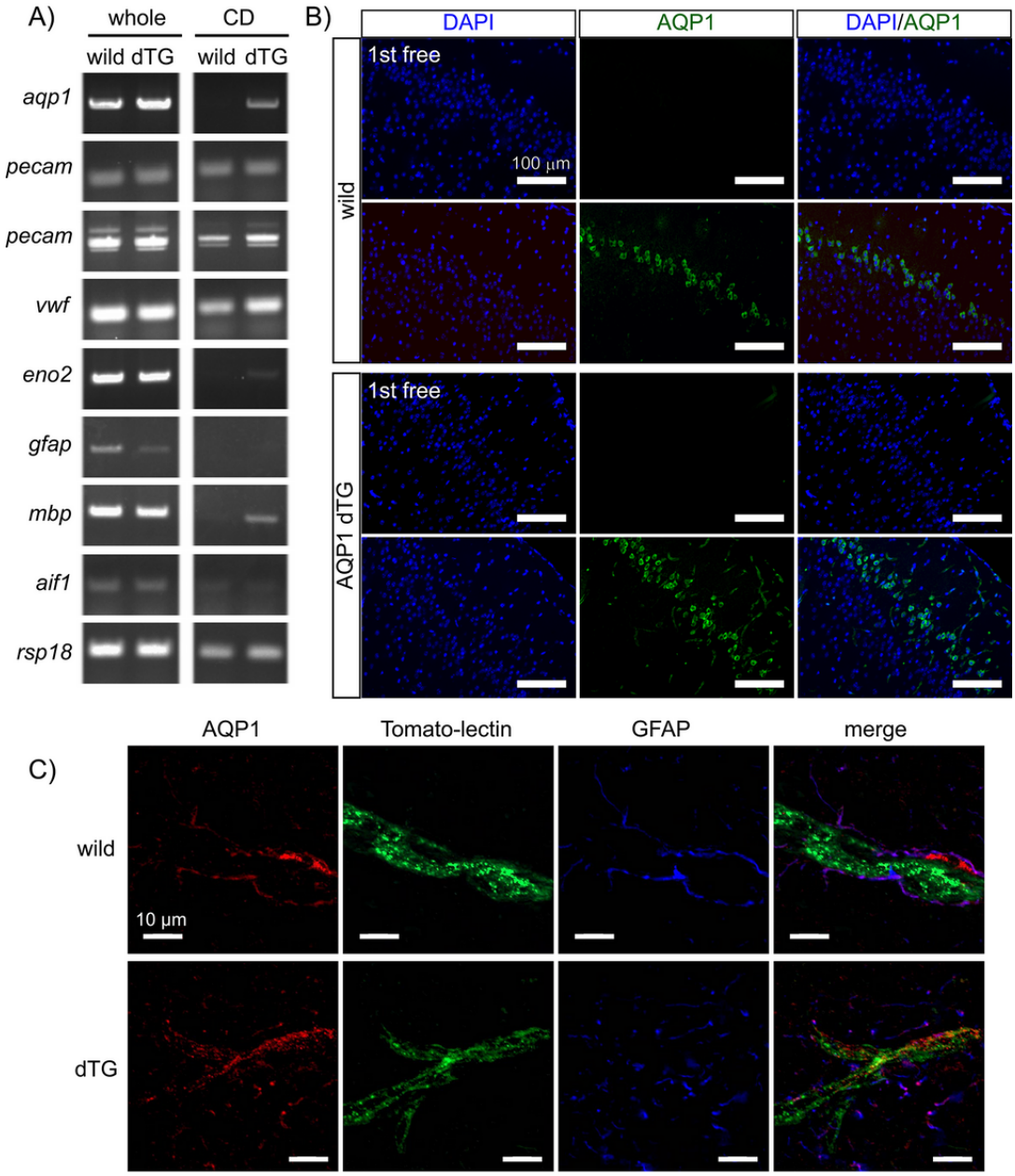

Figure 1

AQP1 expression increases in the endothelial cells (ECs) of Tie2-Cre/LNL-AQP1 dTG mice To evaluate Tie2-Cre/LNL-AQP1 dTG mice with an increased AQP1 expression in ECs under the control of Tie2 promoter, AQP1 was determined in the telencephalon of the brain. (A) Aqp1 expression was ubiquitously detected in the whole brains of wild and Tie2-Cre/LNL-AQP1 dTG mice, and it was not different. After capillary depletion (CD), the expression levels of endothelial marker genes (two different primer sets of pecam and vwf) and housekeeping gene (rsp18) were similar in both the wild and dTG mice. However, the expression of aqp1 was greater in dTG than in wild mice. Whole brain fractions were also detected in neuronal (eno2), astroglial (gfap), oligodendroglial (mpb), and microglial (iba1) sections, but they were decreased or not detected in CD fractions, suggesting that CD fractions are rich in ECs. (B) Immunofluorescence staining for AQP1 in the brain demonstrated that AQP1 immunoreactions in dTG were detected in the vessels, in addition to the neurons of piriform cortex. (C) Multiple-staining of AQP1, endothelial (Tometo-lectin), and astroglial (GFAP) markers were used to determine whether AQP1 immunoreactions were well merged with tomato-lectin in dTG.

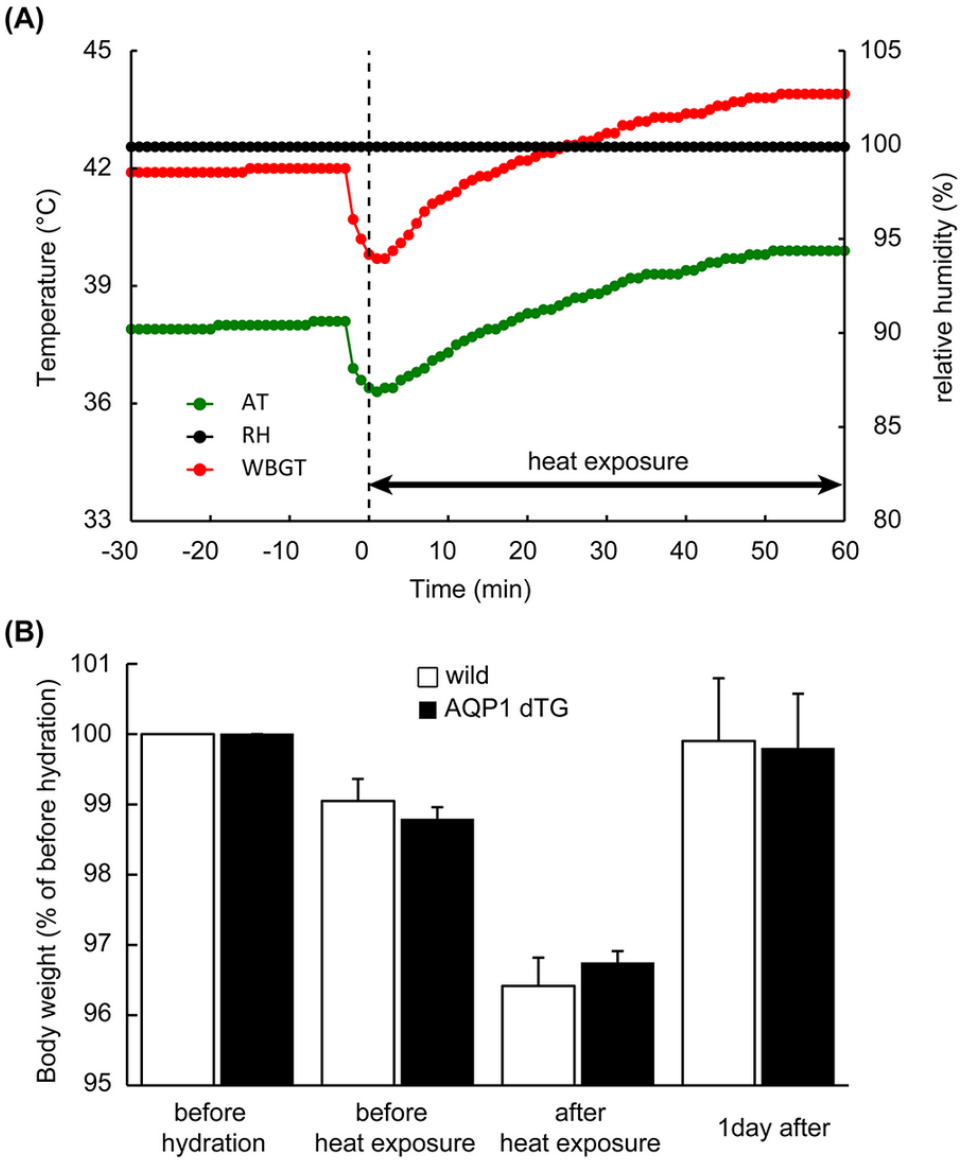

Figure 2

Condition of heat stroke model and body weight (BW) during the experiment (A) Transition of ambient temperature (AT), relative humidity (RH), and wet bulb globe temperature (WBGT) before and during heat exposure. AT and RH inside the chamber were 38.1 °C and >99.9%, and WBGT was calculated at 42 °C. AT and WBGT temporally decreased when the animals were dropped into the chamber, and after 60 min, AT and WBGT gradually increased and finally reached 39.9 and 43.9 °C, respectively. (B) Compared to the BWs before hydration, which was 100 %, after 1 h of heat exposure they decreased and returned mostly to basal levels after one day of heat exposure. No significant difference was observed in BW during the experimental periods.

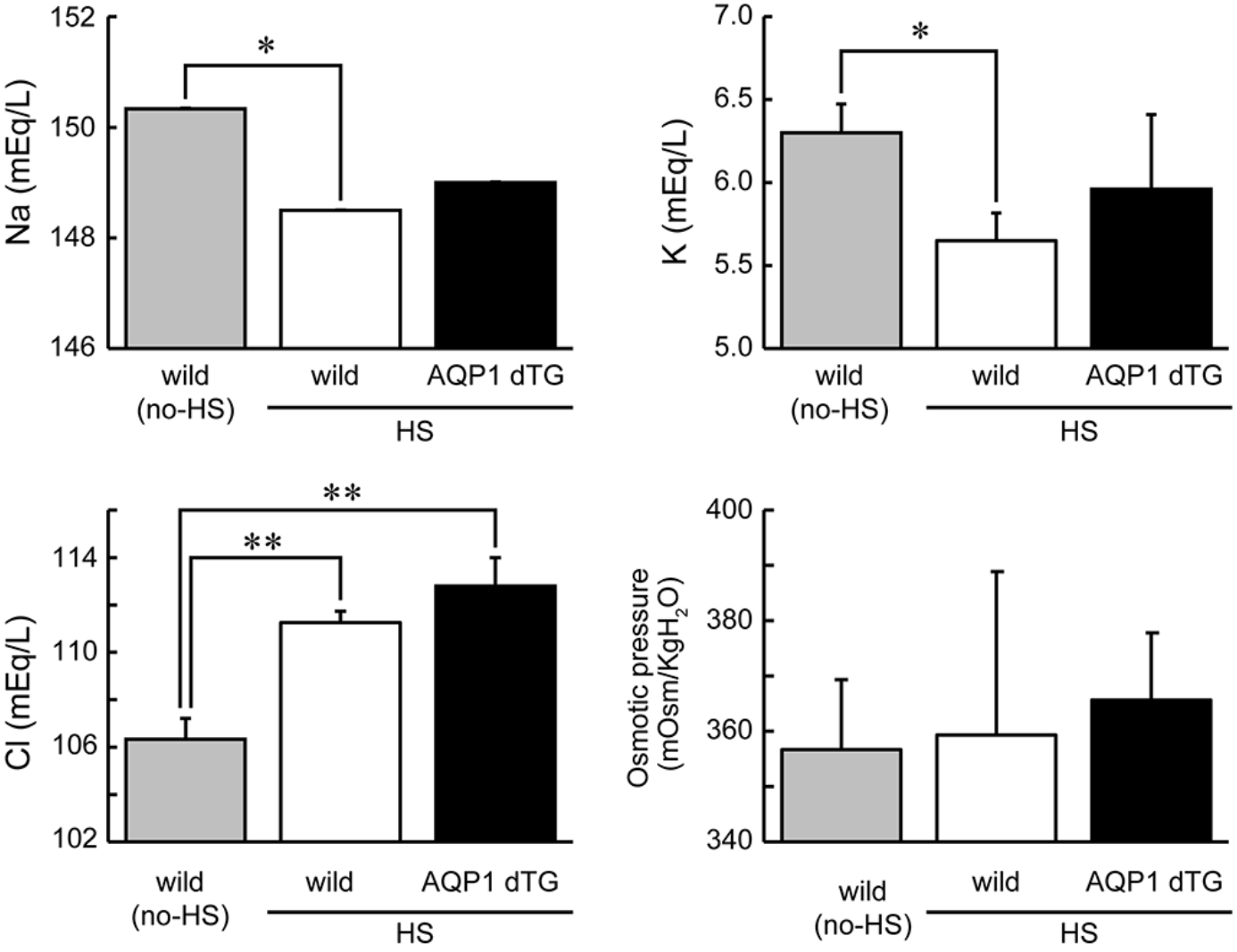

Figure 3

Serum electrolytes and osmotic pressures one day after heat exposure Levels of Na+ (A), K+ (B), Cl- (C), and osmotic pressures (D) determined in wild (wild; n=4) and Tie2-Cre/LNL-AQP1 dTG (AQP1 dTG; n=5) mice. Na+ and K+ were decreased and Cl- increased in both heat-exposed groups as compared to those in non-heat-exposed (no-HS) wild animals (n=3). Data are expressed as the mean ± SE. *p<0.05, **p<0.01 (Tukey's post hoc test).

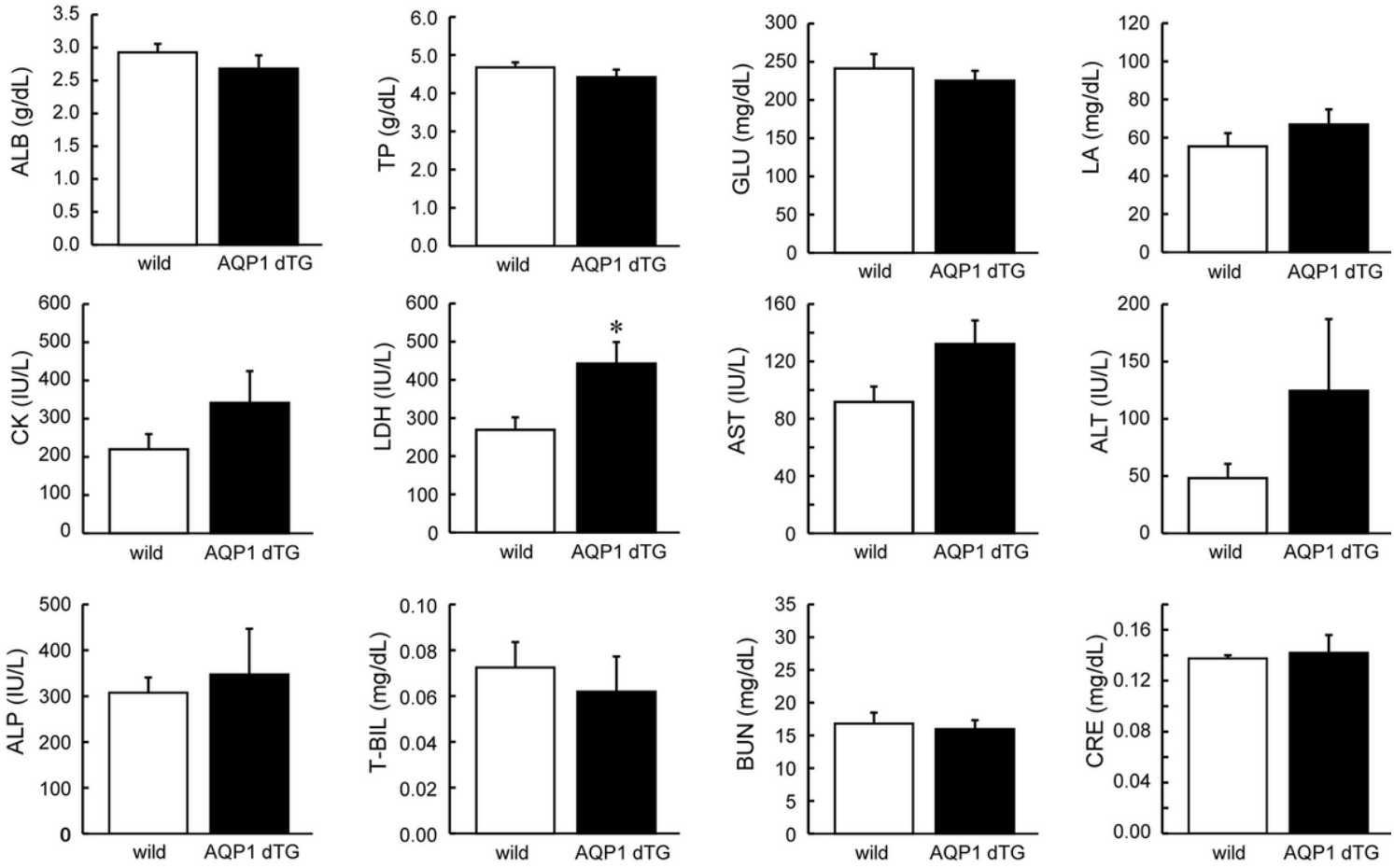

Figure 4

Comparison of serum biochemical parameters, including tissue damage markers Serum biochemical parameters were determined after one day of heat exposure. Lactate dehydrogenase (LDH), a tissue damage marker, was significantly higher in Tie2-Cre/LNL-AQP1 dTG mice (n=5) than in wild-type mice (n=4; $p<0.05$). Data are expressed as the mean ± SE. *$p<0.05$ (Student's t-test).

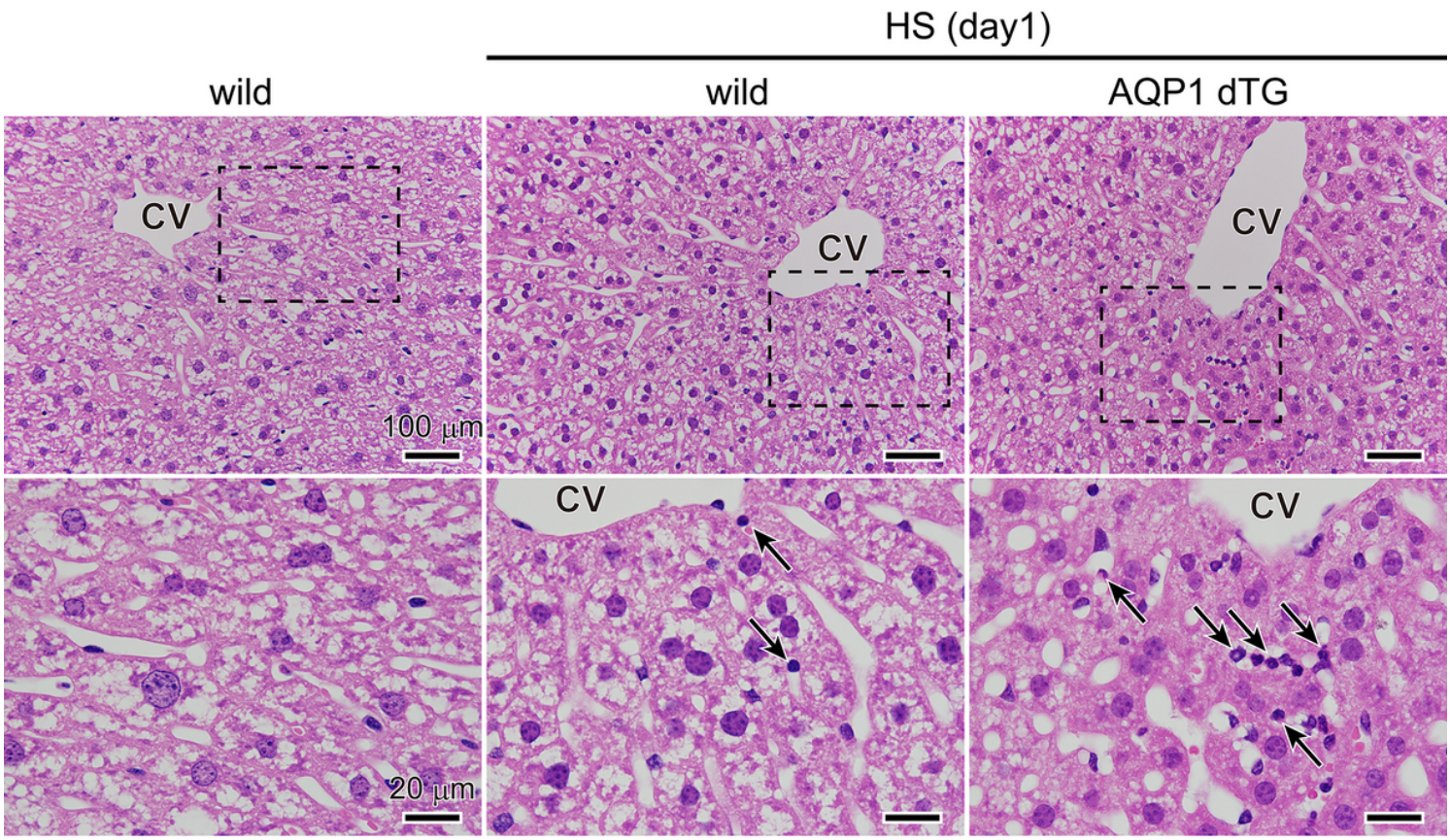

Figure 5

Morphological comparison of the liver Representative images of the livers after hematoxylin-eosin staining in the non-heat-exposed and heat-exposed wild and Tie2-Cre/LNL-AQP1 dTG (AQP1 dTG) mice. High-magnification images of each rectangle are shown at the bottom of each image. Leukocytes are observed after heat exposure (arrows). CV: central vein of hepatic lobules.

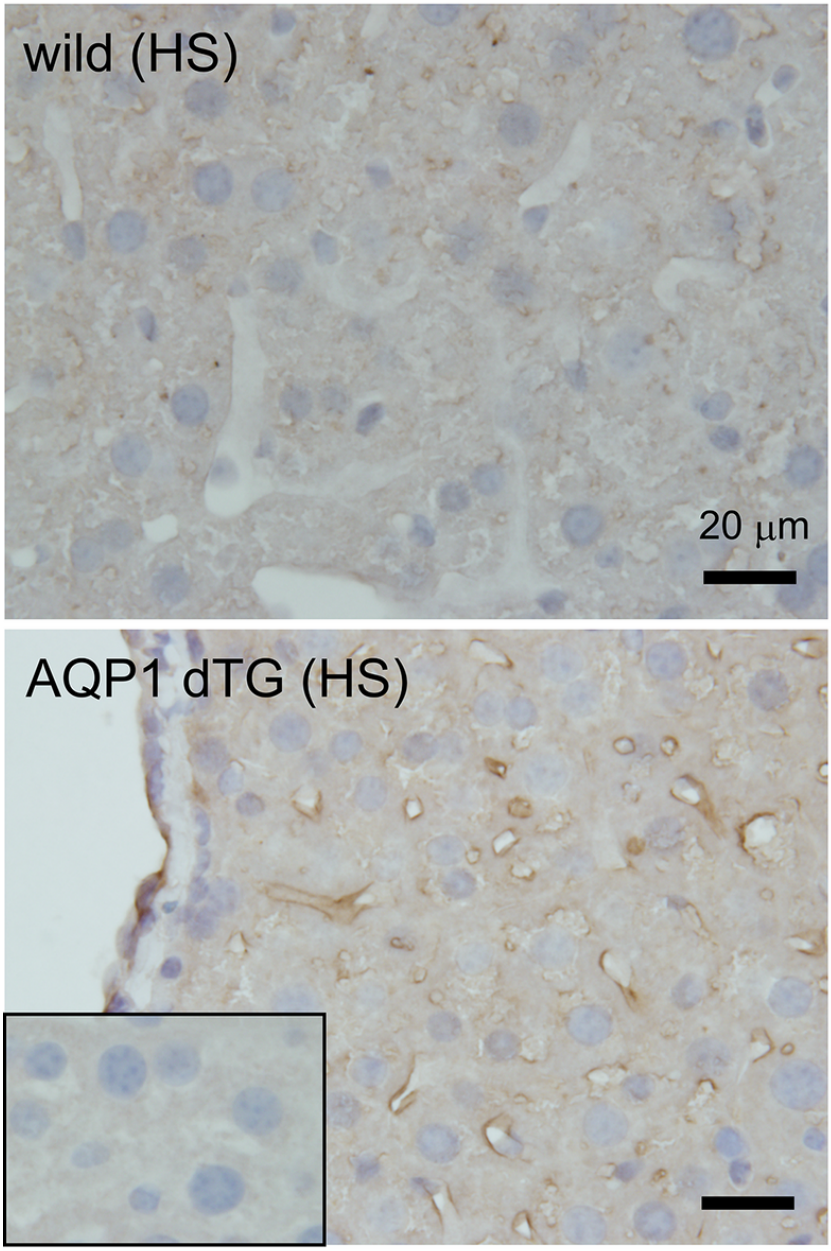

Figure 6

3-nitrotyrosine (3-NT) immunostaining in the liver A proteinic oxidative metabolite, 3-NT, was immunostained in the liver after one day of heat exposure. Minimal or no staining was observed in the primary antibody-free negative control (1st AB-free NC; inset of bottom) in the liver of Tie2-Cre/LNL-AQP1 dTG mice. 3-NT-ir was slightly detected in wild mice (top), and it was prominent in the vessels, including sinusoids of the livers in Tie2-Cre/LNL-AQP1 dTG (AQP1 dTG) mice (bottom).

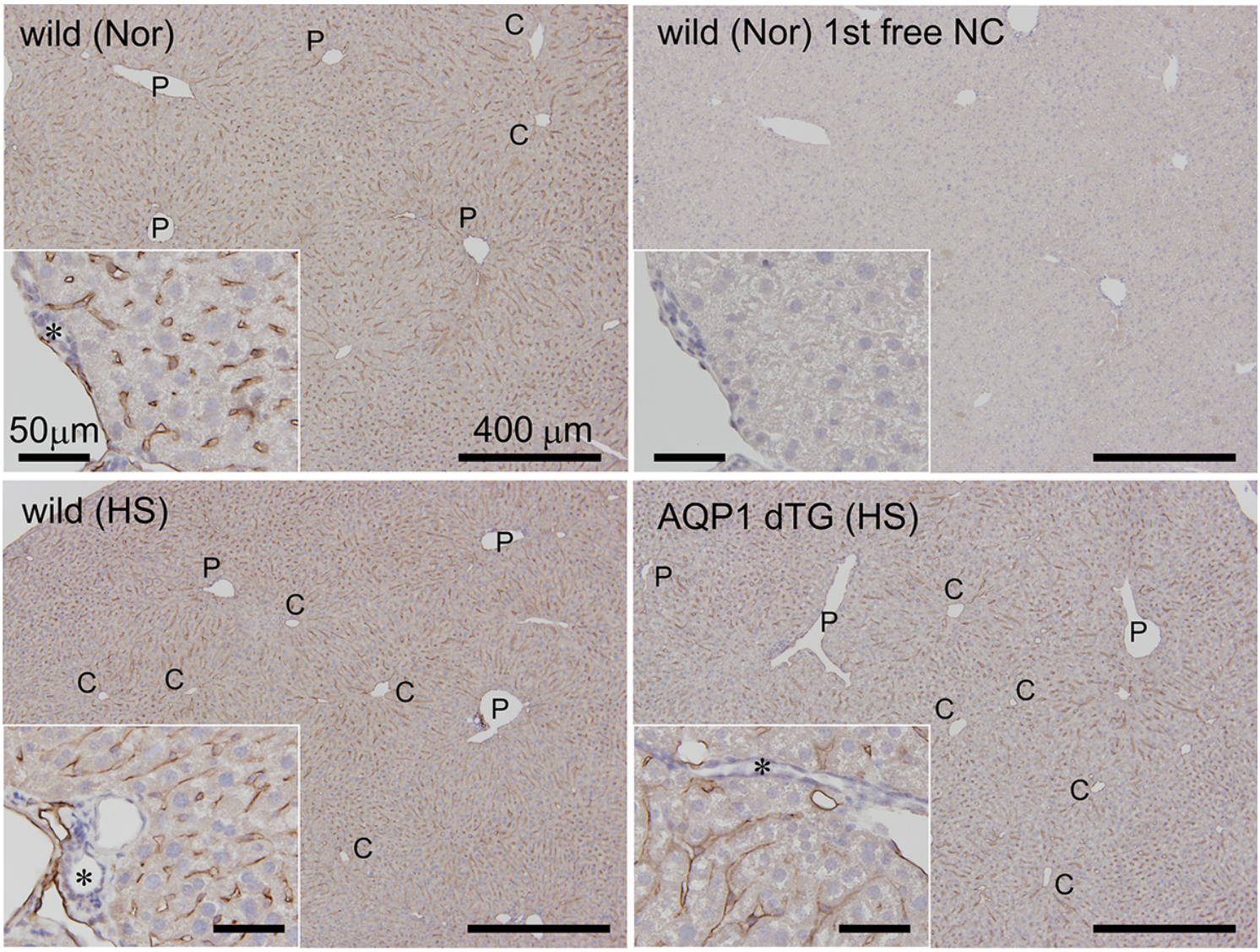

Figure 7

AQP1 immunostaining in the liver AQP1 immunostaining was performed in the livers of wild mice with/without heat exposure and Tie2-Cre/LNL-AQP1 dTG (AQP1 dTG) mice. AQP1-ir was ubiquitously observed in the hepatic vasculatures, including the sinusoids of non-heat-exposed wild mice (Nor), and AQP1-ir showed no staining in the hepatocytes and small bile ducts (asterisk) of portal triads (inset). No or few staining was observed in the primary antibody free negative control (1st AB free NC) in the liver of wild mice (Nor). The stainabilities of AQP1-ir were not drastically different between the wild (HS) and Tie2-Cre/LNL-AQP1 dTG (HS) mice after heat exposure. C: central vein of hepatic lobules; P: portal triad.

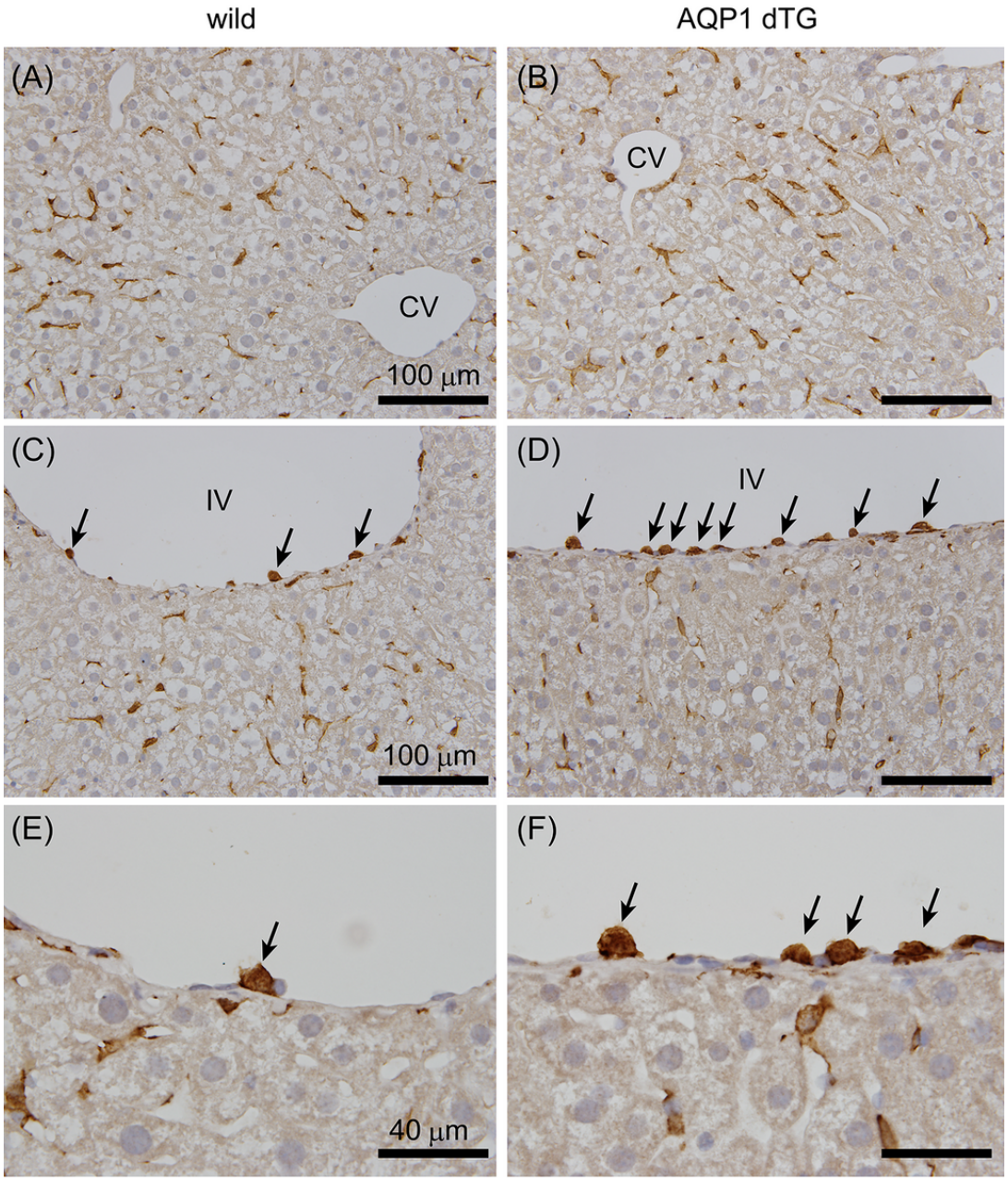

Figure 8

Iba1 immunostaining in the liver The red-brown colored Iba1-ir was observed in the sinusoids, suggesting the presence of Kupffer cells, and it did not drastically differ between the wild (A) and Tie2-Cre/LNL-AQP1 dTG (AQP1 dTG, B) mice. Iba1-ir (arrows) was also recognized in the small-and medium-sized vessels, such as the interlobular vessels (IV), and it was more prominent in Tie2-Cre/LNL-AQP1 dTG (D and F) mice than in wild mice (C and E). (E) and (F) are high magnification images of Iba1-positive reactions on IV. CV, central vein; IV, interlobular vessel; scale bars, 100 μm (A-D) and 40 μm (E and F).

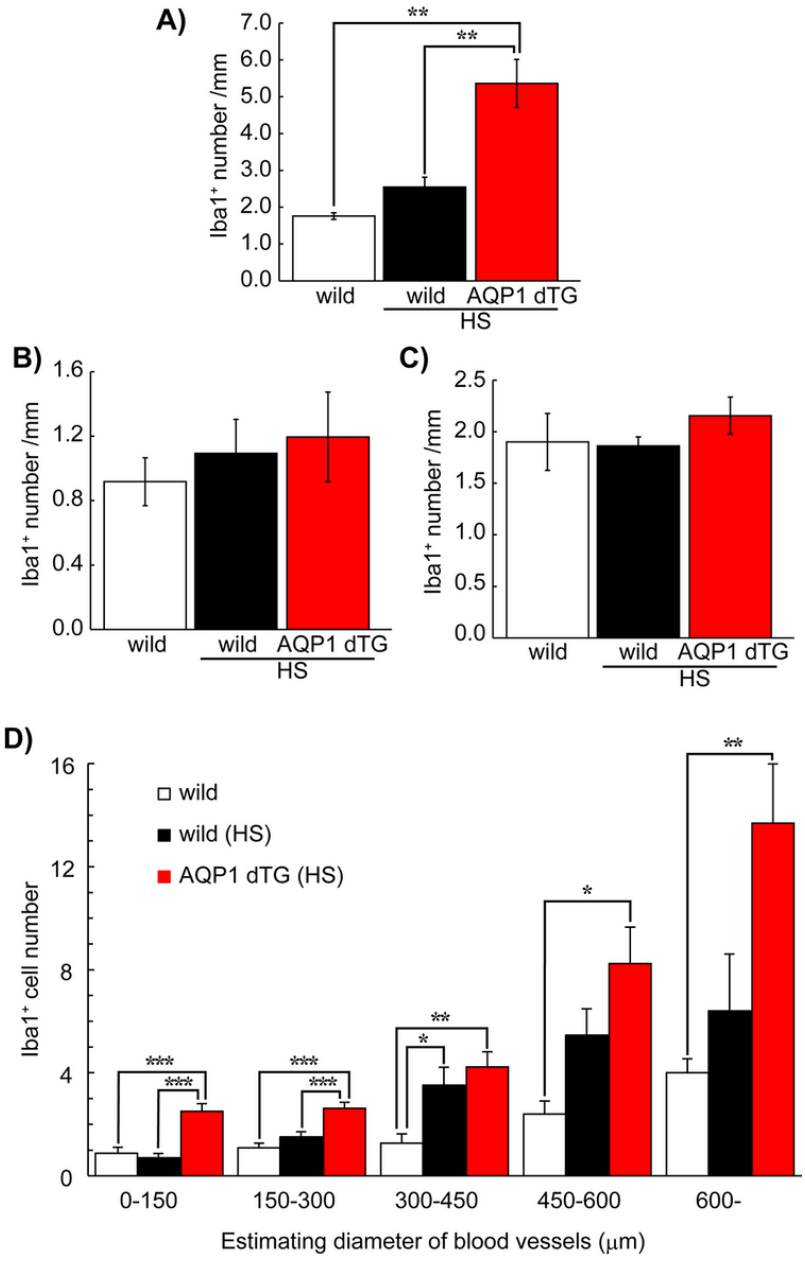

Figure 9

Comparison of Iba1-positive numbers on the blood vessels of the liver Vasculature adherent Iba1-positive cells (Iba1+) were counted in 30 vessels of the liver (A) and brain (B) and 20 - 24 vessels of the kidney (C) in each animal, and they were expressed as the mean number and length of the vessel (mm). (A) Iba1+ numbers were significantly higher in Tie2-Cre/LNL-AQP1 dTG mice (n=5) than in wild mice both with (n=4) and without (n=3) heat exposure. The numbers were not different between the brain and kidney. (D) Iba1+ number in the liver was compared to estimate the diameter of each blood vessel, which was calculated from the circumferential length. While Iba1+ numbers in Tie2-Cre/LNL-AQP1 dTG mice were greater in any vessel, the diameters of 0-150 and 150-300 μm significantly differed from the wild mice after heat exposure. The data are expressed as mean ± SE. *p<0.05, **p<0.01, ***p<0.001 (Tukey's post hoc test).

Supplementary Files

This is a list of supplementary files associated with this preprint. Click to download.

- ARRIVEComplianceQuestionnaireFINAL.pdf